Catalysis Science & Technology

The dynamic behavior of dilute metallic alloy Pd_xAu_{1-x}/SiO_2 raspberry colloid templated catalysts under CO oxidation

Journal:	*Catalysis Science & Technology*
Manuscript ID	CY-ART-03-2021-000469.R1
Article Type:	Paper
Date Submitted by the Author:	25-Apr-2021

Complete List of Authors:	Filie, Amanda; Harvard University, John A. Paulson School of Engineering and Applied Sciences Shirman, Tanya; Harvard University, John A. Paulson School of Engineering and Applied Sciences Aizenberg, Michael; Harvard University, John A. Paulson School of Engineering and Applied Sciences Aizenberg, Joanna; Harvard University; Harvard University, Department of Chemistry and Chemical Biology Friend, Cynthia; Harvard University, Chemistry and Chemical Biology; Harvard University, John A. Paulson School of Engineering and Applied Sciences Madix, Robert; Harvard University, School of Engineering and Applied Science

ARTICLE

The dynamic behavior of dilute metallic alloy Pd_xAu_{1-x}/SiO_2 raspberry colloid templated catalysts under CO oxidation

Received 00th January 20xx,
Accepted 00th January 20xx

DOI: 10.1039/x0xx00000x

Amanda Filie,[a] Tanya Shirman,[a] Michael Aizenberg,[a] Joanna Aizenberg,[a,b] Cynthia M. Friend,[a,b] and Robert J. Madix[a*]

Dilute palladium-in-gold alloys have potential as efficient oxidation catalysts; controlling the Pd surface distribution is critical. Here, the activity for CO oxidation catalyzed by robust dilute Pd-in-Au nanoparticles supported on raspberry-colloid-templated (RCT) silica depends on the pretreatment and gas environment. The activities of oxygen-pretreated catalysts are different in light-off studies versus after long-term use. Transient increases in activity are also induced by flowing CO/He at 553 K. Altogether, these results indicate changes in Pd distribution at the surface induced by reactive gases and that light-off studies alone are not adequate for evaluation of alloy catalyst performance. Kinetic studies show evidence of both isolated and multiple Pd atoms. A dual-site mechanism is operative over $Pd_{0.02}Au_{0.98}$ RCT-SiO_2, whereas a single-site mechanism governs reaction over $Pd_{0.10}Au_{0.90}$ RCT-SiO_2. The distinct mechanisms suggest that tuning the ratio of isolated to clustered Pd sites is possible, underscoring the importance of characterization under reaction conditions.

1. Introduction

Bimetallic alloy nanoparticles have been extensively studied for use in catalysis. The most widely studied bimetallic alloys consist of combinations of Group VIII and Group IB metals, with particular interest in the combinations of Ni-Cu and Pd-Au for hydrogenation, dehydrogenation, hydrogenolysis and isomerization.[1–3] Beginning with these studies, alloying effects on catalytic activity and selectivity were classified as having two origins: 1) the electronic interactions between the metal atoms, or so-called "ligand effects", and 2) the structural organization of the two metal atoms at the surface, or so-called "geometric effects."[4] Until recently most research was focused on binary alloys containing relatively large fractions of each metal with the objective of altering the electronic properties of the entire alloy. More recently studies of binary systems in which there is a minor amount of one component, so-called dilute binary alloys (in the limit, single atom alloys) have begun, and different principles therefore have arisen. For example, a relatively reactive metal can be incorporated into a relatively inactive host, producing catalytic behavior inaccessible to either metal alone.[5–13] More specifically, the minority species may provide a critical reaction step such as the activation of oxygen[14,15] or hydrogen[9,16,17] that initiates a selective reaction sequence on the surface of the less reactive metal, as observed for selective oxidation of alcohols on Ag/Au dilute binary alloys,[13] selective hydrogenation of 1-hexyne on Pd/Au single atom alloys,[8] and selective hydrogenation of butadiene on Pt/Cu single atom alloys.[9]

Binary alloys of Pd and Au have indeed been extensively studied, with particular attention toward introducing Au to a predominantly Pd-based system to mitigate over-oxidation. Palladium/gold catalysts have been explored for vinyl acetate synthesis,[18–21] CO oxidation,[22–26] and H_2O_2 synthesis,[27–31] usually with alloy compositions above 50 at% Pd. Various effects have been reported; for example, the importance of specific Pd-Pd ensembles to enhance formation of vinyl acetate has been suggested;[21] the creation of a Pd shell over a Au core was proposed to enhance the activity of supported PdAu nanoparticles on alumina for H_2O_2 synthesis due to electronic promotion of the activity of Pd layers at the surface.[30] In many of these earlier studies the nanoparticles were largely non-uniform, sometimes consisting of pure Au, pure Pd, and PdAu alloy particles, making it difficult to draw conclusions on the effects of particle composition.[22–24] On the other hand, model surface science studies with either alloy single crystal PdAu(100) or evaporated thin films of Pd and Au highlight the effects of different states of aggregation of Pd at the surface.[14,15,20,21,32] Both ligand and geometric effects were invoked to explain catalyst performance at low concentrations of Pd. Very little research has been done, however, in the dilute binary alloy nanoparticles limit.

Because of the potential of binary PdAu catalysts for selectively catalyzing oxidation reactions, understanding the nature of oxygen activation by their surfaces is important. The degree of the assembly of the Pd atoms at the surface of a PdAu alloy appears to strongly affect dioxygen dissociation at the

[a] John A. Paulson School of Engineering and Applied Sciences, Harvard University, Cambridge, MA 02138, USA.
[b] Department of Chemistry and Chemical Biology, Harvard University, Cambridge, MA 02138, USA.

† Footnotes relating to the title and/or authors should appear here.
Electronic Supplementary Information (ESI) available: [details of any supplementary information available should be included here]. See DOI: 10.1039/x0xx00000x

surface. It is well known that metallic gold does not dissociate O_2,[33–35] whereas O_2 readily dissociates on Pd surfaces.[36–38] Previous work demonstrates such activation on binary PdAu alloy surfaces; clusters of contiguous Pd atoms at the surface of the PdAu alloy activate molecular O_2, whereas isolated Pd atoms do *not* dissociate O_2.[14,39,40] Further, the dissociation barrier for molecular O_2 decreases as the Pd coverage increases.[41] This effect is attributed to the decrease in the dissociation barrier as Pd(111) islands develop, in agreement with earlier results obtained from temperature programmed desorption and density functional theory (DFT).[40] Tuning the distribution of Pd atoms at the surface thus may significantly affect the activity and selectivity of these alloy catalysts.

Partly because the reaction mechanism of CO oxidation is simple, it has served as a useful test reaction for the factors determining the catalytic behavior of PdAu alloy catalysts (as well as a large number of other alloy systems). Reaction between CO and dioxygen is facile on clean single crystal surfaces of Pd and undetectable on Au. Also, pure Pd nanoparticles catalysts are generally reported to be much more active for CO oxidation than those of pure Au nanoparticles when loaded onto an inert support,[22,24] though the activity measured for pure Au nanoparticles is inconsistent in the literature.[23] Most of the studies on supported PdAu alloy nanoparticles are for Pd content above approximately 50 wt%. Methods of preparation vary, and tests of the activity often rely on so-called "light-off" curves of the as-prepared catalysts.[22–24,42] The combination of these factors appears to produce substantial variability in performance, making comparison of different studies difficult.

It is possible to synthesize dilute binary alloy nanoparticle catalysts with a narrow size distribution of uniform composition. It also appears feasible to tune the surface composition to optimize its reactivity through either electronic effects, geometric effects or both.[43–46] The gaseous environment, bulk alloy composition, and temperature significantly affect the surface composition and may be used to tune selectivity or activity.[45–48] For example, theoretical calculations indicate that CO-Pd and Pd-O complexes energetically stabilize segregation of Pd atoms to the surface of the alloy, whereas adsorbed H drives Pd toward the bulk.[46,49,50] Accordingly, rapid cooling of a dilute PdAu nanoparticle catalyst after pretreatment in CO or O_2 at elevated temperature significantly increases the activity for 1-hexyne hydrogenation due to Pd stabilized at the catalyst surface.[46] Surface science studies of $Au_{30}Pd_{70}(110)$[51] and supported PdAu[29,30,52] nanoparticle catalysts also clearly show enrichment of Pd at the surface after high temperature O_2 treatment. Further, gas phase CO pretreatment of a AuPd single crystal can be used to alter the distribution of Pd ensembles at the surface; low pressure of CO tends to form only isolated Pd atoms at the surface, while higher pressures lead to the formation of both isolated Pd atoms and contiguous Pd sites.[14,15,32] Since the surface coverage of each reactant plays a critical role in determining the kinetics of oxidation, reactant-induced segregation of the active metal may strongly affect the rate of CO oxidation in these dilute alloys.[32]

Highly dilute Pd-in-Au nanoparticles containing 2 at% and 10 at% Pd supported on a raspberry-colloid-templated silica support (designated Pd_xAu_{1-x} RCT-SiO_2 where x = atomic fraction of Pd) were found to be active for CO oxidation, with the "light-off" temperature for the reaction decreasing as Pd content increases.[42] Herein, we demonstrate the dynamic nature of Pd-dilute Pd_xAu_{1-x} RCT-SiO_2 catalysts for CO oxidation and the sharp dependence of reaction kinetics and mechanism on the bulk Pd concentration – even in the dilute limit. Moreover, the activity of the $Pd_{0.02}Au_{0.98}$ RCT-SiO_2 changes significantly *after* "light-off" under reaction conditions, but it can be conditioned thermally to achieve a stable state. The kinetics of the CO and O_2 reaction, both the dependence on reactant partial pressures and activation energy, on $Pd_{0.10}Au_{0.90}$ RCT-SiO_2 are identical to that on pure Pd catalysts, indicating the role of Pd ensembles at this Pd concentration, but suggest electronic modification of the surface Pd by the underlying Au. In contrast, the kinetic parameters of $Pd_{0.02}Au_{0.98}$ RCT-SiO_2 suggest a bifunctional, dual site mechanism, which utilizes both isolated Pd atoms and clustered Pd ensembles. These studies illustrate the potential to tune the surface composition of Pd_xAu_{1-x} RCT-SiO_2 to adjust catalyst performance in different reactions.

2. Methods

2.1. Material Synthesis

The alloy catalysts, $Pd_{0.02}Au_{0.98}$ RCT-SiO_2 and $Pd_{0.10}Au_{0.90}$ RCT-SiO_2 (also referred to as 2% PdAu and 10% PdAu throughout the text), were prepared using a previously reported method.[42] Briefly, monometallic Au nanoparticles (NPs) were first formed[53] by adding aqueous trisodium citrate and sodium borohydride ($NaBH_4$) to a vigorously stirred solution of $HAuCl_4$ and H_2O. This method produced Au NPs with a narrow size distribution with an average size of approximately 5 nm in diameter. The Pd_xAu_{1-x} bimetallic nanoparticles (where x = atomic fraction of Pd) were prepared using a previously published procedure;[54] different quantities of palladium (II) nitrate hydrate ($Pd(NO_3)_2$) were added to a solution containing 40 mL of as-synthesized Au NPs and 5 mL of 0.1 ascorbic acid aqueous solution and stirred for 12 hours at room temperature. The NPs were loaded onto a silica oxide matrix using a raspberry colloid templated (RCT) approach previously reported.[42,55] First, they were added to a solution of thiol-modified polystyrene colloids to form so-called "raspberry colloids." These colloids formed an ordered assembly of spheres via water evaporation. A silica precursor was added to the assembly, back-filling the interstitial spaces between the colloidal spheres. The back-filled colloid assembly was then calcined in air at 773 K for 2 h to remove the polystyrene colloids and solidify the silica support, producing a highly ordered SiO_2 matrix with partially embedded nanoparticles (RCT-SiO_2). The material after this initial calcination and before any further pretreatments is referred to as the "as-prepared" state.

2.2. Ex-situ Characterization

Inductively coupled plasma mass spectrometry (ICP-MS) was used to determine the total metal loading and average alloy

nanoparticle composition of the catalysts (Table 1). Scanning electron microscopy (SEM) was employed to confirm the highly ordered nature of the catalysts. Transmission electron microscopy (TEM) was used to determine the nanoparticles size distribution and confirm the metal loading and dispersion of nanoparticles throughout the support material.

Table 1. The total metal loading, as percent total weight of nanoparticles on the silica support, and the atomic percent of Pd in the PdAu alloy nanoparticles as determined by inductively coupled plasma mass spectrometry (ICP-MS) of the as-prepared catalysts (Agilent Technologies 7700x Inductively Coupled Plasma Mass Spectrometer).

RCT-SiO_2 Catalyst	Metal Loading (wt %)	Concentration of Pd (at % Pd)
Au	9.2	N/A
$Pd_{0.02}Au_{0.98}$	11.6	2.1 ± 0.4
$Pd_{0.10}Au_{0.90}$	12.3	9.5 ± 1.1

2.3. Catalyst size distribution, dispersion and stability

The PdAu alloy catalysts studied here exhibited good particle dispersion, a narrow size distribution, and excellent thermal stability (Fig. 1). Changes in the size distributions of both $Pd_{0.02}Au_{0.98}$ and $Pd_{0.10}Au_{0.90}$ RCT-SiO_2 catalysts were minimal following extended use at temperatures up to 598 K (Fig. 1A and 1F, respectively). After use, the average nanoparticle size for the as-prepared $Pd_{0.02}Au_{0.98}$ RCT-SiO_2 increased only from 5.8 ± 1.4 nm to 8.3 ± 4.0 nm, and the size distribution broadened, whereas the average nanoparticle size and distribution of the $Pd_{0.10}Au_{0.90}$ RCT-SiO_2 increased only slightly (from 6.1 ± 2.1 nm to 7.3 ± 3.0 nm). SEM images of the highly ordered structures of the catalysts as-prepared and post-catalysis after numerous high temperature treatments followed by catalytic testing were very similar and showed minimal changes in the support structure (Fig. 1). The metal loading of the catalysts is evident in the TEM images of both the as-prepared and used catalysts.

2.4. Catalytic Measurements

Catalytic activity and selectivity were measured in a gas-phase flow reactor at atmospheric pressure. Mass flow controllers supplied ultra-high purity oxygen (Airgas, 99.994%), ultra-high purity helium (Airgas, 99.999%) and a 10% CO/90% He mixture (Airgas, 10% ± 0.2% CO, balance He) to the reactor. The reactor tube was housed in a temperature-controlled furnace sufficiently long to maintain constant temperature throughout the catalyst bed. A thermocouple, contained in a glass sheath, was inserted into the top of the catalyst bed to monitor its temperature. The as-prepared catalyst was crushed and sieved to restrict the catalyst particles' size between 100-300 µm. Catalyst beds were prepared by diluting the sieved catalyst powder with quartz sand particles with diameters between 210-300 µm. The catalyst-sand mixture was transferred to a quartz reactor tube (1cm inner diameter) fitted with a glass frit, resulting in a catalyst bed height of 1 cm. Quartz wool plugs were placed before and after the catalyst bed to mix reactant gases and to minimize the loss of catalyst powder. The compositions of the catalysts tested were monometallic Au, 2.1 atomic % Pd in Au ($Pd_{0.02}Au_{0.98}$) and 9.5 atomic % Pd in Au ($Pd_{0.10}Au_{0.90}$). A single catalyst bed of each composition was prepared and used in the experiments testing for sensitivity to gas environments and for kinetic studies. The reactor effluent was analyzed using the thermal conductivity detector of an online gas-chromatograph (Agilent 7890A) equipped with a CARBONPLOT column. The concentration of CO_2 in the reactor effluent was measured to quantify the rate of CO_2 formation, which was normalized by total mass of precious metal in the catalyst bed (Supplementary Information, section S.1).

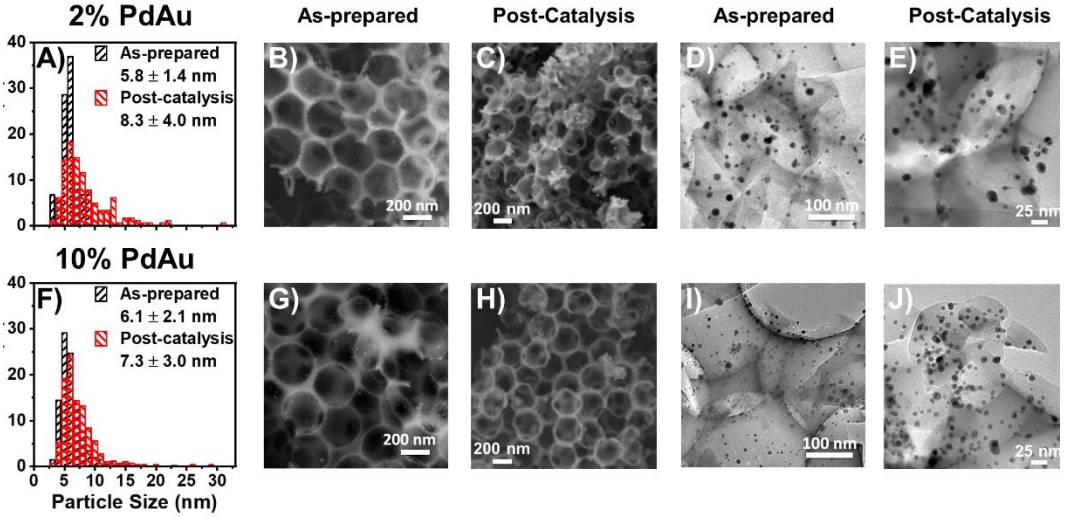

Figure 1. The Pd_xAu_{1-x} RCT-SiO_2 catalysts are thermally stable. (A) The nanoparticle size distribution of as-prepared and post-catalysis 2% PdAu changed minimally after nine pretreatments at 773 K followed by catalyst testing for CO oxidation - approximately 224 h of catalyst testing in total between 423 K and 598 K. The thermal stability was further corroborated by the persistently ordered silica support and well-dispersed nanoparticles observed in representative SEM (Zeiss, FESEM Ultra55) and TEM (JEOL 2100) images, respectively, of the 2% PdAu catalyst (B,D) as-prepared and (C,E) post-catalysis. Similarly, (F) the nanoparticle size distribution of 10% PdAu as-prepared and post-catalysis remained approximately the same after seven pretreatments followed by catalyst testing – approximately 80 h in total between 373 K and 573 K. (G,H) SEM and (I,J) TEM images of the material in either state showing the material unchanged at the length scales shown.

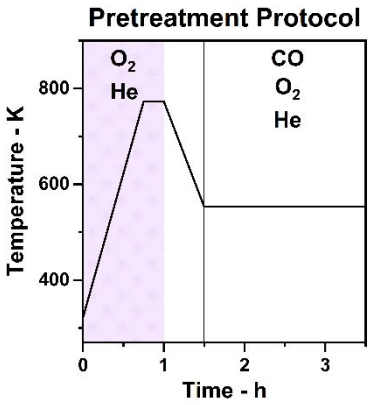

Scheme 1. Schematic illustrating the pretreatment of the catalysts prior to measuring activity. (The total flow rate was 50.0 sccm when heating in O_2/He mixture to 773 K and 25.0 sccm when reacting in mixture of CO/O_2/He at 553 K, GHSV of 3,800 hr^{-1} and 2,000 hr^{-1} respectively.)

Prior to measuring catalytic activity, the catalysts were pretreated in oxygen (20% O_2, balanced with He, total flow rate of 50.0 sccm, gas hourly space velocity (GHSV) of 3,800 hr^{-1}), heated from 323 K to 773 K at a rate of 10 K/min, and then held at 773 K for 15 minutes. This catalyst is referred to as the "O_2 - pretreated" state. The O_2 - pretreated catalyst was then cooled in He to either 423 K or 553 K, where the catalyst was held under reaction conditions until its activity reached a steady-state under a standard set of conditions (5% CO, 10% O_2, balanced with He, total flow rate of 25.0 sccm, GHSV of 2,000 hr^{-1}) (Scheme 1).

The effect of either ambient CO or O_2 on the catalysts was investigated by interrupting the flow of one of the reactants for a fixed period of time. After one hour under standard reaction conditions, O_2 flow was discontinued, exposing the catalyst to a 5% CO environment for approximately 30 minutes. O_2 was re-introduced for one hour and the steady state activity monitored. Thereafter, the CO flow was shut-off, exposing the catalyst to a 10% O_2 environment for approximately 40 minutes. CO was re-introduced and the approach to steady state under the standard reaction conditions was monitored.

3. Results

3.1. Conditioning of the $Pd_{0.02}Au_{0.98}$ RCT-SiO_2 catalyst by thermal cycling under reaction conditions after light-off

The steady state activity of the O_2 - pretreated $Pd_{0.02}Au_{0.98}$ RCT-SiO_2 catalyst for CO oxidation was enhanced by thermal cycling, ultimately reaching a stable, conditioned state (Fig. 2A). The catalyst was initially heated stepwise from 523 K to 563 K to reach steady state at each temperature (Fig. 2A). The rate increase with temperature yielded an apparent activation energy of 106 ± 5 kJ/mole in excellent agreement with our previous light-off studies (Fig. S1).[42] Subsequently, the temperature was retraced downward, yielding an activity greater that the first set of measurements and a lower apparent activation energy of 80 ± 3 kJ/mole (Fig. 2A). Repetition of the thermal cycling produced a stable catalytic activity with an

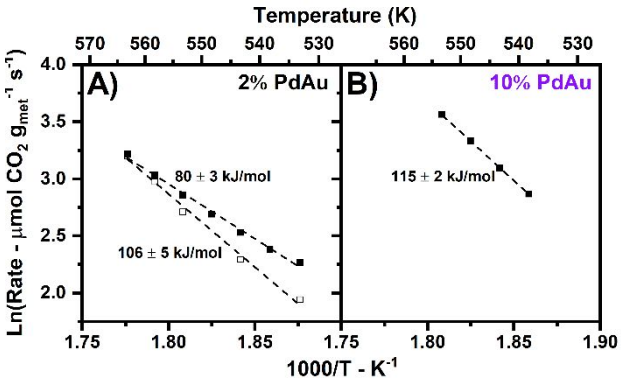

Figure 2. Arrhenius plots for the activation energies of the 2% and 10% PdAu RCT catalysts. (A) The apparent activation energy observed over the 2% PdAu catalyst decreased significantly when cycling the reaction temperature from 523 K to 563 K: (□) initially increasing temperature; (■) retracing temperature downward. (B) The apparent activation energy over the 10% PdAu catalyst measured when cycling the reaction temperature from 553 K to 538 K (■) after it was stabilized under reaction conditions at 553 K for 2 – 3 h. Reaction conditions: 523 K ≤ Temperature ≤ 563 K; 5% CO, 10% O_2, balanced with He; Total flow rate = 25.0 sccm; Gas hourly space velocity = 2,000 hr^{-1}. Catalysts: m_{cat} = 36.0 mg of $Pd_{0.02}Au_{0.98}$ RCT-SiO_2, metal loading = 11.6 wt%; m_{cat} = 40.0 mg of $Pd_{0.10}Au_{0.90}$ RCT-SiO_2, metal loading = 12.3 wt%.

activation energy of ~80 kJ/mole (Fig. S1, Table S1). This conditioned state persisted for reactions with various CO and O_2 mixtures and changes in the reaction temperature between 538 K and 553 K; its isothermal activity remained constant over several hours of operation.

A similar conditioned state could also be achieved by cooling the O_2 - pretreated $Pd_{0.02}Au_{0.98}$ RCT-SiO_2 catalyst to 553 K, stabilizing its activity at that temperature under reaction conditions, and conducting 3 sequential temperature ramps between 553 K and 538 K (Fig. 3). After 3 cycles of cooling and heating, the apparent activation energy stabilized at 85 ± 3 kJ/mole (Fig. S2, Table S2). The two treatments, although begun at different temperatures, apparently resulted in a similar state of the catalyst. The same treatment was performed on the $Pd_{0.10}Au_{0.90}$ RCT-SiO_2 catalyst to achieve a stable activity (Fig. 3) to yield an apparent activation energy of 115 kJ/mol (Fig. 2B).

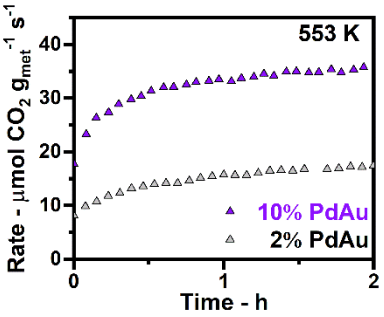

Figure 3. Initial stabilization of the O_2 pretreated PdAu catalysts under reaction conditions. The rate of CO_2 formation increased smoothly toward steady state over the 2% PdAu and 10% PdAu catalysts over a period of 2 h in the break-in period, suggesting that the composition of the surface changed significantly. Reaction conditions: Temperature = 553 K; 5% CO, 10% O_2, balanced with He; Total flow rate = 25.0 sccm; Gas hourly space velocity = 2,000 hr^{-1}. Catalysts: m_{cat} = 36.0 mg of $Pd_{0.02}Au_{0.98}$ RCT-SiO_2, metal loading = 11.6 wt%; m_{cat} = 40.0 mg of $Pd_{0.10}Au_{0.90}$ RCT-SiO_2, metal loading = 12.3 wt%.

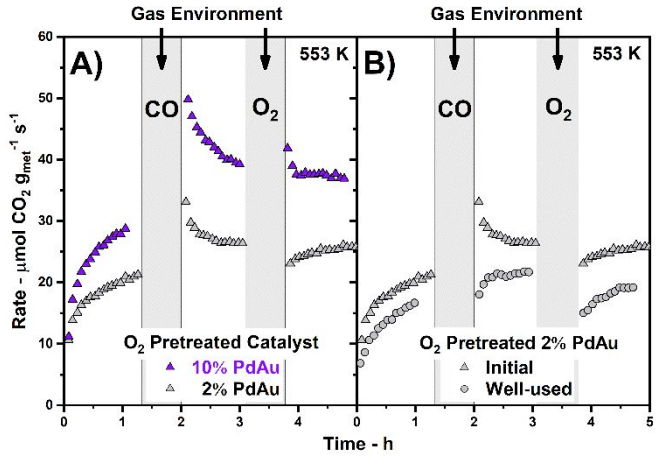

Figure 4. The activity of the dilute Pd-in-Au catalysts approached a steady-state under reaction conditions, regardless of the state of the catalyst and independent of transient changes in the gas environment. (A) The CO/He environment initially increased the activity of both the 2% PdAu and 10% PdAu by a factor of ~1.6. Subsequent exposure to O_2/He did not change the steady-state activity. (B) The rate of CO_2 formation over the O_2 - pretreated 2% PdAu catalyst, both in its initial and well-used state, as it was subjected to changes in the reactant environment approached steady-state activity. CO environment: 5% CO, balanced with He; Total flow rate = 25.0 sccm. O_2 environment: 10% O_2, balanced with He; Total flow rate = 25.0 sccm. Reaction conditions: Temperature = 553 K; 5% CO, 10% O_2, balanced with He; Total flow rate = 25.0 sccm; Gas hourly space velocity = 2,000 hr^{-1}. Catalysts: m_{cat} Initial $Pd_{0.02}Au_{0.98}$ = 40.0 mg, m_{cat} Well-used $Pd_{0.02}Au_{0.98}$= 36.0 mg, metal loading = 11.6 wt%; m_{cat} $Pd_{0.10}Au_{0.90}$ = 40.0 mg, metal loading = 12.3 wt%.

3.2. The effects of reaction conditions on activity during the activation period

The activities of both the O_2 - pretreated $Pd_{0.02}Au_{0.98}$ and $Pd_{0.10}Au_{0.90}$ RCT-SiO_2 catalysts changed in response to changes in the reactant environment at 553 K (Fig. 4A). Specifically, the activities increased upon exposure to CO, but no O_2, for an increment in time. For example, as the conversion approached steady state in a 5% CO – 10% O_2 reactant mixture, the O_2 flow was interrupted so that the catalysts were exposed to only CO and He for 30 minutes. Upon resumption of O_2 flow the activities of the catalysts increased abruptly to a value of ~1.6 times higher than the steady state, decaying to a value that was ~25% higher after 1 h on stream. In contrast, exposure to O_2 without CO at 553 K only minimally changed the catalyst activity (Fig. 4).

Since the general behavior of the catalysts in reaching steady state activity between initiation of reaction and the final steady state is very similar with or without interruption of the reactant flows (Figs. 3 and 4), it appears the exposure to CO only transiently increases the activity of the catalyst above its ultimate steady state value; in other words, the activity of the catalyst appears to be controlled by the gas phase composition for fresh catalysts. Indeed, after either CO or O_2 exposures alone, the catalysts appear to quickly approach the same steady state activity upon resumption of flow of both reactants (Fig. 4A). Notably, the sensitivity of the catalyst to changes in reactant composition appears to diminish after extended use (Fig. 4B). In this case exposure to CO produces little effect and the activity is lowered by exposure to O_2.

Although the steady state activities of the catalysts at 553 K increase with increasing Pd concentration, they do not increase as much as might be expected. The concentration of the $Pd_{0.10}Au_{0.90}$ RCT-SiO_2 catalyst is 5 times greater than that of the $Pd_{0.02}Au_{0.98}$ RCT-SiO_2 catalyst, but its steady state activity is larger by only a factor of 1.5 – 2.0.

In order to assess the contribution of the gold itself to the activity of the PdAu nanoparticles, comparable studies were performed on pure Au nanoparticle catalysts of the same particle size. The steady state activity of the Au RCT-SiO_2 was substantially lower than that of either Pd-containing catalyst (Fig. S3). Furthermore, the rate of CO oxidation over the gold catalyst exhibited no measurable temperature dependence; its initial activity for CO oxidation simply decreased steadily over eight hours under reaction conditions unlike the $Pd_{0.02}Au_{0.98}$ RCT-SiO_2 (Fig. S4). Also, the conversion over the Au nanoparticle catalyst was insensitive to changes in the gas phase composition during its initial "activation", unlike the Pd-containing catalysts (Fig. S5). The fact that the activity of both Pd-containing catalysts exceeded that of the monometallic Au catalyst (Table 2), signifies the importance of Pd in promoting the reaction, as do the transient effects of CO treatment. So, although the Au may itself contribute some activity to the catalyst the Pd plays the dominant role, even at the lowest Pd concentration studied.

Table 2. The steady-state activity of the O_2 pretreated Au, 2% PdAu, and 10% PdAu catalysts, after testing for sensitivity to oxidative and reducing environments. Reaction conditions: Temperature = 553 K; 5% CO, 10% O_2, balanced with He; Total flow rate = 25.0 sccm; Gas hourly space velocity = 2,000 hr^{-1}. Catalysts: m_{cat} = 40.8 mg of Au RCT-SiO_2, metal loading 9.2 wt%; m_{cat}= 40.0 mg of $Pd_{0.02}Au_{0.98}$ RCT-SiO_2, metal loading = 11.6 wt%; m_{cat} = 40.0 mg of $Pd_{0.10}Au_{0.90}$ RCT-SiO_2, metal loading = 12.3 wt%.

RCT-SiO_2 Catalyst	Rate (μmol CO_2 g_{met}^{-1} s^{-1})
Au	18 ± 1
$Pd_{0.02}Au_{0.98}$	26 ± 1
$Pd_{0.10}Au_{0.90}$	37 ± 1

3.3. Kinetics Orders

The reaction orders for CO and O_2 were determined for the conditioned $Pd_{0.02}Au_{0.98}$ and $Pd_{0.10}Au_{0.90}$ RCT-SiO_2 catalysts between 538 K and 553 K (Fig. 5 and 6, respectively). Over the conditioned $Pd_{0.02}Au_{0.98}$ RCT-SiO_2 catalyst, the rate of CO oxidation at 538 K was independent of CO concentration (i.e., zero order) and first-order in oxygen partial pressure (Figs. 5A and 5B, respectively). These values were reproduced several times.

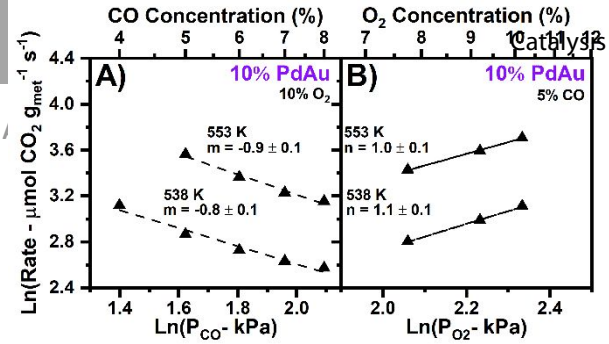

Figure 6. The reaction order dependence of 10% PdAu on CO and O_2 resembled that expected for Pd-based catalysts. (A) The reaction order of CO and (B) O_2 were determined by changes in the rate of CO_2 production per mass of metal in 10% PdAu as the inlet partial pressure of carbon monoxide and oxygen were varied, respectively, at 538 K and 553 K. Conversions were kept below 25%. Reaction conditions: kinetic studies on CO, 5 - 8% CO, 10% O_2, balanced with He; kinetic studies of O_2, 5% CO, 7.5-10% O_2 concentrations, balanced with He. Total flow rate of 25.0 sccm; m_{cat} = 40.0 mg $Pd_{0.10}Au_{0.90}$ RCT-SiO_2, metal loading = 12.3 wt%.

determined by changes in the rate of CO_2 production per mass of metal in 10% PdAu as the inlet partial pressure of carbon monoxide and oxygen were varied, respectively, at 538 K. Conversions were kept below 25%. Reaction conditions: kinetic studies on CO, 5 - 8% CO, 10% O_2, balanced with He; kinetic studies of O_2, 5% CO, 7.5-10% O_2 concentrations, balanced with He. Total flow rate of 25.0 sccm; m_{cat} = 36.0 mg RCT $Pd_{0.02}Au_{0.98}$ RCT-SiO_2, metal loading =11.6 wt%.

For comparison, experiments were conducted on the $Pd_{0.10}Au_{0.90}$ RCT-SiO_2 catalyst (Fig. 6). Under standard reaction conditions the rate of CO_2 formation per gram of metal was approximately 52 % greater than that observed on the catalyst containing 2% Pd, consistent with previous measurements (Table 2). For the $Pd_{0.10}Au_{0.90}$ RCT-SiO_2 catalyst, which showed clear evidence of Pd clustering at the surface,[42] the reaction orders observed were essentially minus one for CO and one for O_2 (Fig. 6A and B, respectively).

4. Discussion

We have recently demonstrated that monometallic Pd RCT-Al_2O_3 catalysts are very robust,[56] remaining non-sintered and highly active in oxidation of carbon monoxide and hydrocarbons after prolonged exposure to aggressive reaction streams at temperatures as high as ~1073 K. The novel bimetallic dilute Pd-in-Au RCT-SiO_2 catalysts reported here likewise exhibit remarkable robustness, with only minimal sintering after subjecting them to seven to nine O_2 pretreatments at 773 K followed by testing for CO oxidation. The $Pd_{0.02}Au_{0.98}$ RCT-SiO_2 catalyst was tested for approximately 224 h between 423 K and 598 K, and the $Pd_{0.10}Au_{0.90}$ RCT-SiO_2 catalyst was examined for approximately 80 h between 373 K and 573 K. No increase in the median particle diameter for the $Pd_{0.02}Au_{0.98}$ RCT-SiO_2 catalyst, and an increase of only 20% (5.0 nm to 6.0 nm) for the $Pd_{0.10}Au_{0.90}$ RCT-SiO_2 catalyst was measured using TEM (Fig. 1). On the other hand, the particle size distribution of the $Pd_{0.02}Au_{0.98}$ RCT-SiO_2 catalyst shows the formation of numerous particles between 10 and 20 nm, resulting in an increase of the *average* particle size from 5.8 nm to 8.3 nm. The average particle size of the $Pd_{0.10}Au_{0.90}$ RCT-SiO_2 catalyst remained nearly constant (Fig. 1). These dilute alloy RCT catalysts show remarkable resistance to sintering, even though the composition of each NP is very nearly pure gold. This stability is attributed to the nature of the raspberry colloid structuring of the silica matrix, which results in partial embedding of the particles.[57] This assertion is supported by prior studies showing that nanoparticles attached but not embedded in the silica sinter significantly.[42]

Both dilute Pd-in-Au alloy catalysts examined in this work form homogenous alloys,[42] and they remain homogeneous after many hours of use; however, the surface composition changes with ambient conditions and temperature. Pd has a higher surface free energy than Au, causing preferential segregation of Pd into the bulk of the pure material; however, binding of either CO or O with the Pd at the surface can cause segregation to the surface, since both CO and O bond more strongly to Pd than to Au, based on DFT studies.[46,58,59] In fact, such segregation has been reported in Pd-in-Au alloys for both oxygen[51] and carbon monoxide environments,[15] including for a $Pd_{0.04}Au_{0.96}$ RCT-SiO_2 catalyst.[46] Therefore, the pretreatment of the catalysts in oxygen at 773 K must draw Pd to the surface. Indeed previous studies of PdAu catalysts supported on Al_2O_3 that were calcined in air report the formation of PdO.[60] Since the reaction mixture contains both CO and O_2, the surface would be expected to reach a condition determined by the balance of the interactions of the Pd with both gases. Exposure of the catalyst to either gas alone could perturb this steady state condition and lead to transient changes in the activity for CO oxidation, as observed here (Fig. 4). Unfortunately, due to the low concentration of Pd in these catalysts the Pd distribution between bulk and surface cannot as of yet accurately be determined by EXAFS measurements.[42]

An important result of our work is the demonstration that light-off tests of the activity of catalysts with different alloy compositions, taken alone, may *not* indicate their relative activity under steady state conditions because of changes in the catalyst during long-term operation. The initial light-off of the O_2 -pretreated $Pd_{0.02}Au_{0.98}$ RCT-SiO_2 catalyst showed an apparent activation energy of 106 – 110 kJ/mol for CO oxidation,[42] nearly identical to that of pure Pd catalysts.[42] The initially high activation energy observed in the light-off of the $Pd_{0.02}Au_{0.98}$ RCT-SiO_2 catalyst can be attributed to excess Pd at the surface due to the high temperature pretreatment in O_2. The 20 kJ/mole reduction in activation energy on the fully conditioned catalysts at steady state (Fig. 2 and Fig. S1) suggests a change in the surface concentration of Pd as a result of extended reaction, since the particle structure appears unchanged by extended reaction cycles. Changes in surface composition are also supported by the transient changes in catalyst activity induced by exposure to CO only (Fig. 4). The transient increase in activity due to exposure to CO alone may arise from either stabilization of Pd at the surface by CO or by reduction of residual PdO at the surface. Our experiments do not allow us to distinguish these two possibilities. Overall, our results highlight the necessity of conditioning the dilute alloy catalyst to obtain meaningful performance information.

Recent studies show CO effectively stabilizes Pd atoms at the surface of PdAu nanoparticles under specific reaction conditions. Model studies of supported PdAu nanoparticles annealed in ultrahigh vacuum up to 673 K using near ambient pressure X-ray photoelectron spectroscopy reveal that CO oxidation reaction conditions enrich the surface with Pd through CO adsorption-induced segregation of Pd atoms

without the formation of Pd oxide at the surface.[61,62] Furthermore, the Pd-CO complex that forms at room temperature decomposes at temperatures of 473 K and above, either through CO desorption[61] or reaction with O_2.[62] This temperature is coincident with that at which we first observed CO_2 to form in our flow reactor studies, implying that inhibition by adsorbed CO may be operative in our experiments at lower temperature.

Also, whether the Pd atoms at the surface are isolated or clustered determines if molecular oxygen dissociatively adsorbs. Isolated Pd atoms have been shown to be incapable of activating molecular oxygen;[14] hence, one must conclude that under reaction conditions Pd clusters must be present on both the $Pd_{0.02}Au_{0.98}$ and $Pd_{0.10}Au_{0.90}$ RCT-SiO_2 catalysts. However, room temperature CO diffuse reflectance infrared Fourier transform spectroscopy (DRIFTS) measurements, taken after H_2 *reduction* of the as-prepared catalysts by H_2 at 523 K for 1 h, indicate the presence of only isolated Pd atoms at the surface of the $Pd_{0.02}Au_{0.98}$ RCT-SiO_2 catalyst but shows evidence for both single Pd and Pd clusters on the $Pd_{0.10}Au_{0.90}$ RCT-SiO_2 catalyst.[42]

The seeming difference in these DRIFTS results can be attributed to the effects that CO, O_2 and H_2 pretreatments have on the Pd distribution. Recent work indicates that Pd migrates into the bulk of the $Pd_{0.02}Au_{0.98}$ RCT-SiO_2 catalyst during hydrogen pretreatment but segregates to the surface in either a CO or O_2 atmosphere at reaction temperatures.[46,61,62] Pd clusters would not be expected at the surface after hydrogen reduction, whereas they may be present after either treatment in CO or O_2. These results demonstrate the importance of performing DRIFTS or other surface sensitive experiments that probe ensemble size under reaction conditions to evaluate the Pd configuration, as previously suggested.[61] Similar effects have been reported recently for the dehydrogenation of ethanol over dilute Pd/Au nanoparticle catalysts.[63] Pd segregation to the surface in the presence of CO is supported by several previous DFT studies.[46,63,64]

Though the fact that the catalyst with both very dilute (2%) and moderate (10%) Pd alloy compositions catalyze CO oxidation, implying an important role of contiguous Pd atoms at the surface, their different dependencies on the partial pressures of the reactants suggest substantially different mechanisms. The reaction orders determined for the $Pd_{0.10}Au_{0.90}$ RCT-SiO_2 catalyst, as well as the activation energy measured, agree with those reported previously for Pd single crystals,[65,66] model silica-supported Pd catalysts,[67] and Pd nanoparticle catalysts[68,69] (see below) suggesting that the $Pd_{0.10}Au_{0.90}$ RCT-SiO_2 catalyst behaves much like Pd metal, even after extended use. Previous work shows that a contiguous monolayer of Pd on a single crystal surface of Au (Au(111)) shows chemical properties similar to bulk Pd, binding CO with the same strength as on a pure Pd(111) surface.[70,71] These results clearly suggest the involvement of large Pd clusters on the surface of the $Pd_{0.10}Au_{0.90}$ RCT-SiO_2 alloy catalyst in the oxidation of CO.

4.1. Single active site LH mechanism:

The most widely accepted reaction mechanism for CO oxidation on Pd is the Langmuir-Hinshelwood mechanism.[72] The elementary steps are summarized below for the case of a single active site (*) that competes for binding both CO and O_2.

$$CO_{(gas)} + * \rightleftarrows CO^* \quad (1)$$

$$O_{2(gas)} + * \rightarrow O_2^* \quad (2)$$

$$O_2^* + * \rightarrow O^* + O^* \quad (3)$$

$$CO^* + O^* \rightarrow CO_2^* + * \quad (4)$$

$$CO_2^* \rightarrow CO_{2(gas)} + * \quad (5)$$

Following Nibbelke et al[73] and others,[74] if O_2 chemisorption is rate limiting and adsorbed CO is the most abundant surface species, the rate expression for the rate of CO_2 production, R (Eq. 1), becomes

$$R = \frac{2k_2^f P_{O_2}}{K_1 P_{CO}} \quad \text{(Eq. 1)}$$

where k_2^f is the rate constant for oxygen chemisorption, and K_1 is the ratio of rate constants for CO adsorption and desorption.[73] This mechanism yields a partial pressure dependence in CO of minus one, a partial pressure dependence in O_2 of plus one, and an apparent activation energy similar to energy barrier for CO desorption from Pd.[75,76]

The apparent activation energy observed over the $Pd_{0.10}Au_{0.90}$ RCT-SiO_2 catalyst (115 ± 2 kJ/mol) studied here is close to the activation energy observed in previous light-off studies of Pd RCT-SiO_2 (119 ± 5 kJ/mol)[42] and of model silica-supported Pd catalysts (104.6 kJ/mol to 113.0 kJ/mol).[77] The agreement between the kinetics observed on the $Pd_{0.10}Au_{0.90}$ RCT-SiO_2 catalyst and pure Pd is thus consistent with the presence of Pd clusters at the surface of the $Pd_{0.10}Au_{0.90}$ nanoparticle that imbue the catalyst with Pd-like character.[42] However, the activity of this catalyst is still far below that of a comparable catalyst with similarly sized pure Pd nanoparticles.

4.2. Bifunctional active site LH kinetics:

Guidance for understanding the mechanism on the $Pd_{0.02}Au_{0.98}$ RCT-SiO_2 catalyst is provided by the previous work of Goodman et al.[14,15,32] Using model PdAu bulk alloys and evaporated films with *in situ* infrared spectroscopy Goodman related the state of aggregation of Pd at the surface to the rates of CO oxidation.

They showed that (1) isolated Pd atoms on the alloy surface do not dissociate dioxygen, (2) under CO oxidation reaction conditions both isolated Pd atoms and Pd clusters exist among the Au atoms at the surface, (3) the isolated Pd atoms remain nearly saturated with CO at reaction pressures between 10 – 70 torr CO and temperatures from 300 – 550 K, whereas the population of CO on the Pd clusters decreases sharply to zero above about 475 K, and (4) at reaction temperatures the concentration of CO on the surface Au atoms is immeasurable. Below we consider the implication of these facts on our observations for the $Pd_{0.02}Au_{0.98}$ RCT-SiO_2 catalyst. These observations are generally consistent with a dual site mechanism for CO oxidation.

The zero-order dependence in CO pressure observed for the $Pd_{0.02}Au_{0.98}$ RCT-SiO_2 catalyst in this study is consistent with CO saturation of the isolated Pd sites. Saturation of the extended Au surface by CO is inconsistent with Goodman's observations. Furthermore, adsorption isosteres for CO bound to Au(110) indicate that the CO coverage on Au would be orders of magnitude below saturation at 0.05 bar and 500 K.[78] Moreover, the 85 kJ/mol binding energy of CO to the isolated surface Pd atoms, as measured by Goodman,[15] strongly suggests that CO saturates the isolated Pd atoms. Since it is also known that *CO does not occupy the Pd clusters* at 550 K and that *O_2 is dissociated only by Pd clusters*, the second site of the pair is proposed to be the Pd clusters; i.e., CO binds to the isolated Pd, and O_2 is dissociated by the Pd clusters.

A *general* form for the rate law for a dual active site mechanism, which separates the roles of the isolated and clustered Pd is suggested in Eq. 2.

$$R = k_{LH}\left(\frac{K_{1,isolated}P_{CO}}{1+K_{1,isolated}P_{CO}}\right)\left(\frac{K_{2,\,cluster}P_{O_2}}{1+K_{CO,cluster}P_{CO}+\,K_{2,cluster}P_{O_2}}\right) \qquad \text{(Eq. 2)}$$

This expression in general allows for (1) reversible CO adsorption on the isolated Pd atom, (2) O_2 activation on the Pd cluster sites and (3) (potentially) CO adsorption on the clusters. This rate law reduces to an expression that is zero order in CO and first order in O_2 if saturation coverage of CO is achieved on the isolated Pd site, the CO concentration on the Pd clusters is low, and the steady state coverage of O_2 on the cluster site is well below saturation (Eq. 3). The experiments by Goodman et al described above support criteria 1 and 2 and also show that the coverage of CO on the clusters is immeasurable under reaction conditions. Thus, $K_{1,isolated}P_{CO} \gg 1$, and $K_{CO,cluster}P_{CO}$ and $K_{2,cluster}P_{O_2} \ll 1$, and the rate expression reduces to Eq. 3, as observed experimentally.

$$R = k_{LH}\,K_{2,cluster}\,P_{O_2} \qquad \text{(Eq. 3)}$$

Clearly this dual site mechanism warrants further study.

Finally, the similar transient response of the O_2 - treated $Pd_{0.02}Au_{0.98}$ and $Pd_{0.10}Au_{0.90}$ RCT-SiO_2 catalysts to CO and O_2 environments (Fig. 4) and their disproportional activities per gram of metal (Table 2) suggests an underlying similarity between the configuration of Pd at their surfaces. The presence of clustered Pd is required to dissociate molecular oxygen and promote activity for CO oxidation, but this would not be expected for 2% Pd randomly distributed at the surface. Further, the steady state activity of the $Pd_{0.10}Au_{0.90}$ RCT-SiO_2 (37 μmol g_{met}^{-1} s^{-1}) was only ~2 times greater than that of the $Pd_{0.02}Au_{0.98}$ RCT-SiO_2 catalyst (25 μmol g_{met}^{-1} s^{-1}) although the Pd content differed by a factor of 5. Also, the $Pd_{0.10}Au_{0.90}$ RCT-SiO_2 catalyst exhibits reactive behavior quite similar to surfaces of bulk Pd. These factors indicate that the reactive gas environment causes an increase in the surface Pd atom population that is not necessarily proportional to the bulk concentration.

5. Conclusions

In this study, we show evidence for the dynamic nature of Pd_xAu_{1-x} RCT-SiO_2 catalysts under reaction conditions for catalytic oxidation. Both O_2 treated $Pd_{0.02}Au_{0.98}$ and $Pd_{0.10}Au_{0.90}$ RCT-SiO_2 catalysts undergo changes under reaction conditions and show transient enhanced activity following exposure to a CO gas environment. Reaction order studies of the $Pd_{0.02}Au_{0.98}$ RCT-SiO_2 catalyst suggests a dual active site mechanism for the reaction and suggests the presence of clusters of Pd at the surface despite the dilute quantity of Pd present in the bulk. On the other hand, on the $Pd_{0.10}Au_{0.90}$ RCT-SiO_2 catalyst the kinetics parallel those observed on bulk Pd surfaces, with the activity moderated by the gold host. In general, the results also indicate that the reactive gas environment results in an enhanced concentration of Pd at the surface which gives these catalyst reactive properties unexpected for the low bulk Pd concentrations. The possibility of constructing dilute Pd-in-Au nanoparticle catalysts with varying amount of isolated Pd and clustered Pd sites under specific reaction conditions advances the concept of using reaction conditions or selected pretreatments to tune the surface composition of dilute binary alloy systems for catalytic behavior.

Author Contributions

Amanda Filie: Methodology, Investigation, Writing - Original Draft, Writing - Review & Editing, Visualization **Tanya Shirman:** Investigation, Resources **Michael Aizenberg:** Supervision **Joanna Aizenberg:** Supervision **Cynthia M. Friend:** Conceptualization **Robert J. Madix:** Conceptualization, Supervision, Project Administration and Lead, Writing - Review & Editing

Conflicts of interest

There are no conflicts to declare.

Acknowledgements

This work was supported as part of the Integrated Mesoscale Architectures for Sustainable Catalysis (IMASC), an Energy Frontier Research Center funded by the U.S. Department of Energy, Office of Science, Basic Energy Sciences under Award # DE-SC0012573. A.F. acknowledges a National Science Foundation Graduate Research Fellowship through the National Science Foundation (Grant No. DGE1745303). Any opinions, findings, and conclusions or recommendations expressed in this material are those of the author(s) and do not necessarily reflect the views of the National Science Foundation.

Notes and references

1 J. H. Sinfelt and J. A. Cusumano, in *Advanced Materials in Catalysis*, eds. J. J. Burton and R. L. B. T.-A. M. in C. Garten, Academic Press, 1977, pp. 1–31.

2 P. W. Reynolds, *J. Chem. Soc.*, 1950, 265–271.

3 J. H. Sinfelt, J. L. Carter and D. J. C. Yates, *J. Catal.*, 1972, **24**, 283–296.

4 F. (Feng) Tao, *Chem. Soc. Rev.*, 2012, **41**, 7977–7979.

5 J. Liu, A. J. R. Hensley, G. Giannakakis, A. J. Therrien, A. Sukkar, A. C. Schilling, K. Groden, N. Ulumuddin, R. T. Hannagan, M. Ouyang, M. Flytzani-Stephanopoulos, J.-S. McEwen and E. C. H. Sykes, *Appl. Catal. B Environ.*, 2021, **284**, 119716.

6 J. Liu, M. B. Uhlman, M. M. Montemore, A. Trimpalis, G. Giannakakis, J. Shan, S. Cao, R. T. Hannagan, E. C. H. Sykes and M. Flytzani-Stephanopoulos, *ACS Catal.*, 2019, **9**, 8757–8765.

7 M. D. Marcinkowski, M. T. Darby, J. Liu, J. M. Wimble, F. R. Lucci, S. Lee, A. Michaelides, M. Flytzani-Stephanopoulos, M. Stamatakis and E. C. H. Sykes, *Nat. Chem.*, 2018, **10**, 325–332.

8 J. Liu, J. Shan, F. R. Lucci, S. Cao, E. C. H. Sykes and M. Flytzani-Stephanopoulos, *Catal. Sci. Technol.*, 2017, **7**, 4276–4284.

9 F. R. Lucci, J. Liu, M. D. Marcinkowski, M. Yang, L. F. Allard, M. Flytzani-Stephanopoulos and E. C. H. Sykes, *Nat. Commun.*, 2015, **6**, 8550.

10 B. Xu, C. G. F. Siler, R. J. Madix and C. M. Friend, *Chem. - A Eur. J.*, 2014, **20**, 4646–4652.

11 B. Xu, R. J. Madix and C. M. Friend, *J. Am. Chem. Soc.*, 2010, **132**, 16571–16580.

12 B. Xu, J. Haubrich, C. G. Freyschlag, R. J. Madix and C. M. Friend, *Chem. Sci.*, 2010, **1**, 310–314.

13 L.-C. Wang, K. J. Stowers, B. Zugic, M. L. Personick, M. M. Biener, J. Biener, C. M. Friend and R. J. Madix, *J. Catal.*, 2015, **329**, 78–86.

14 F. Gao, Y. Wang and D. W. Goodman, *J. Am. Chem. Soc.*, 2009, **131**, 5734–5735.

15 F. Gao, Y. Wang and D. W. Goodman, *J. Phys. Chem. C*, 2009, **113**, 14993–15000.

16 H. L. Tierney, A. E. Baber, J. R. Kitchin and E. C. H. Sykes, *Phys. Rev. Lett.*, 2009, **103**, 246102.

17 W.-Y. Yu, G. M. Mullen and C. B. Mullins, *J. Phys. Chem. C*, 2013, **117**, 19535–19543.

18 E. G. Allison and G. C. Bond, *Catal. Rev.*, 1972, **7**, 233–289.

19 R. Abel, P. Colling, K. Eichler, I. Nicolau and D. Peters, in *Handbook of heterogeneous catalysis*, eds. G. (Gerhard) Ertl, H. Knozinger and J. (Jens) Weitkamp, Wiley-VCH, Weinheim, 1997, p. 2298.

20 M. Chen, D. Kumar, C.-W. Yi and D. W. Goodman, *Science*, 2005, **310**, 291–293.

21 Y. F. Han, J. H. Wang, D. Kumar, Z. Yan and D. W. Goodman, *J. Catal.*, 2005, **232**, 467–475.

22 A. M. Venezia, L. F. Liotta, G. Pantaleo, V. La Parola, G. Deganello, A. Beck, Z. Koppány, K. Frey, D. Horváth and L. Guczi, *Appl. Catal. A Gen.*, 2003, **251**, 359–368.

23 J. Xu, T. White, P. Li, C. He, J. Yu, W. Yuan and Y. Han, *J. Am. Chem. Soc.*, 2010, **132**, 10398–10406.

24 K. Qian and W. Huang, *Catal. Today*, 2011, **164**, 320–324.

25 C. M. Olmos, L. E. Chinchilla, J. J. Delgado, A. B. Hungría, G. Blanco, J. J. Calvino and X. Chen, *Catal. Letters*, 2015, **146**, 144–156.

26 K. Qian, L. Luo, Z. Jiang and W. Huang, *Catal. Today*, 2017, **280**, 253–258.

27 P. Landon, P. J. Collier, A. J. Papworth, C. J. Kiely and G. J. Hutchings, *Chem. Commun.*, 2002, 2058–2059.

28 P. Landon, P. J. Collier, A. F. Carley, D. Chadwick, A. J. Papworth, A. Burrows, C. J. Kiely and G. J. Hutchings, *Phys. Chem. Chem. Phys.*, 2003, **5**, 1917–1923.

29 J. K. Edwards, A. F. Carley, A. A. Herzing, C. J. Kiely and G. J. Hutchings, *J. Catal.*, 2005, **236**, 69–79.

30 B. E. Solsona, J. K. Edwards, P. Landon, A. F. Carley, A. Herzing, C. J. Kiely and G. J. Hutchings, *Chem. Mater.*, 2006, **18**, 2689–2695.

31 J. Pritchard, L. Kesavan, M. Piccinini, Q. He, R. Tiruvalam, N. Dimitratos, J. A. Lopez-Sanchez, A. F. Carley, J. K. Edwards, C. J. Kiely and G. J. Hutchings, *Langmuir*, 2010, **26**, 16568–16577.

32 F. Gao, Y. Wang and D. W. Goodman, *J. Phys. Chem. C*, 2010, **114**, 4036–4043.

33 D. D. Eley and P. B. Moore, *Surf. Sci.*, 1978, **76**, L599–L602.

34 A. G. Sault, R. J. Madix and C. T. Campbell, *Surf. Sci.*, 1986, **169**, 347–356.

35 X. Deng, B. K. Min, A. Guloy and C. M. Friend, *J. Am. Chem. Soc.*, 2005, **127**, 9267–9270.

36 X. Guo, A. Hoffman and J. T. Yates, *J. Chem. Phys.*, 1989, **90**, 5787–5792.

37 G. Zheng and E. I. Altman, *Surf. Sci.*, 2000, **462**, 151–168.

38 B. Klötzer, K. Hayek, C. Konvicka, E. Lundgren and P. Varga, *Surf. Sci.*, 2001, **482–485**, 237–242.

39 F. R. Lucci, L. Zhang, T. Thuening, M. B. Uhlman, A. C. Schilling, G. Henkelman and E. C. H. Sykes, *Surf. Sci.*, 2018, **677**, 296–300.

40 W.-Y. Yu, L. Zhang, G. M. Mullen, G. Henkelman and C. B. Mullins, *J. Phys. Chem. C*, 2015, **119**, 11754–11762.

41 S. Han and C. B. Mullins, *ACS Catal.*, 2018, **8**, 3641–3649.

42 M. Luneau, T. Shirman, A. Filie, J. Timoshenko, W. Chen, A. Trimpalis, M. Flytzani-Stephanopoulos, E. Kaxiras, A. I. Frenkel, J. Aizenberg, C. M. Friend and R. J. Madix, *Chem. Mater.*, 2019, **31**, 5759–5768.

43 V. Ponec and G. C. Bond, *Catalysis by Metals and Alloys*,

1995, vol. 95.
44 W. M. H. Sachtler and R. A. Van Santen, *Adv. Catal.*, 1977, **26**, 69–119.
45 M. Luneau, T. Shirman, A. C. Foucher, K. Duanmu, D. M. A. Verbart, P. Sautet, E. A. Stach, J. Aizenberg, R. J. Madix and C. M. Friend, *ACS Catal.*, 2020, **10**, 441–450.
46 M. Luneau, E. Guan, W. Chen, A. C. Foucher, N. Marcella, T. Shirman, D. M. A. Verbart, J. Aizenberg, M. Aizenberg, E. A. Stach, R. J. Madix, A. I. Frenkel and C. M. Friend, *Commun. Chem.*, 2020, **3**, 1–9.
47 A. Wittstock, V. Zielasek, J. Biener, C. M. Friend and M. Baumer, *Science*, 2010, **327**, 319–323.
48 T. Déronzier, F. Morfin, M. Lomello and J.-L. Rousset, *J. Catal.*, 2014, **311**, 221–229.
49 B. Zhu, G. Thrimurthulu, L. Delannoy, C. Louis, C. Mottet, J. Creuze, B. Legrand and H. Guesmi, *J. Catal.*, 2013, **308**, 272–281.
50 V. Soto-Verdugo and H. Metiu, *Surf. Sci.*, 2007, **601**, 5332–5339.
51 M.-C. Saint-Lager, M.-A. Languille, F. J. Cadete Santos Aires, A. Bailly, S. Garaudee, E. Ehret and O. Robach, *J. Phys. Chem. C*, 2018, **122**, 22588–22596.
52 J. K. Edwards, A. F. Carley, A. A. Herzing, C. J. Kiely and G. J. Hutchings, *Faraday Discuss.*, 2008, **138**, 225–239.
53 K. C. Grabar, K. J. Allison, B. E. Baker, R. M. Bright, K. R. Brown, R. G. Freeman, A. P. Fox, C. D. Keating, M. D. Musick and M. J. Natan, *Langmuir*, 1996, **12**, 2353–2361.
54 Y. Ding, F. Fan, Z. Tian and Z. L. Wang, *J. Am. Chem. Soc.*, 2010, **132**, 12480–12486.
55 E. Shirman, T. Shirman, A. V. Shneidman, A. Grinthal, K. R. Phillips, H. Whelan, E. Bulger, M. Abramovitch, J. Patil, R. Nevarez and J. Aizenberg, *Adv. Funct. Mater.*, 2018, **28**, 1704559.
56 T. Shirman, T. J. Toops, E. Shirman, A. V. Shneidman, S. Liu, K. Gurkin, J. Alvarenga, M. P. Lewandowski, M. Aizenberg and J. Aizenberg, *Catal. Today*, 2020, **360**, 241–251.
57 J. E. S. van der Hoeven, S. Kraemer, S. Dussi, T. Shirman, C. H. Rycroft, D. C. Bell, C. M. Friend and J. Aizenberg, *in preparation*.
58 K. G. Papanikolaou, M. T. Darby and M. Stamatakis, *J. Phys. Chem. C*, 2019, **123**, 9128–9138.
59 H. Y. Kim and G. Henkelman, *ACS Catal.*, 2013, **3**, 2541–2546.
60 Z. Suo, C. Ma, M. Jin, T. He and L. An, *Catal. Commun.*, 2008, **9**, 2187–2190.
61 A. V Bukhtiyarov, I. P. Prosvirin, A. A. Saraev, A. Y. Klyushin, A. Knop-Gericke and V. I. Bukhtiyarov, *Faraday Discuss.*, 2018, **208**, 255–268.
62 M. Mamatkulov, I. V Yudanov, A. V Bukhtiyarov, I. P. Prosvirin, V. I. Bukhtiyarov and K. M. Neyman, *J. Phys. Chem. C*, 2019, **123**, 8037–8046.
63 M. Ouyang, K. G. Papanikolaou, A. Boubnov, A. S. Hoffman, G. Giannakakis, S. R. Bare, M. Stamatakis, M. Flytzani-Stephanopoulos and E. C. H. Sykes, *Nat. Commun.*, 2021, **12**, 1549.
64 M. Mamatkulov, I. V Yudanov, A. V Bukhtiyarov and K. M. Neyman, *Nanomaterials*, 2021, 11.
65 J. Szanyi, W. K. Kuhn and D. W. Goodman, *J. Phys. Chem.*, 1994, **98**, 2978–2981.
66 P. J. Berlowitz, C. H. F. Peden and D. W. Goodman, *J. Phys. Chem.*, 1988, **92**, 5213–5221.
67 X. Xu and D. W. Goodman, *J. Phys. Chem.*, 1993, **97**, 7711–7718.
68 N. W. Cant, P. C. Hicks and B. S. Lennon, *J. Catal.*, 1978, 372–383.
69 Y. Li, Y. Yu, J. G. Wang, J. Song, Q. Li, M. Dong and C. J. Liu, *Appl. Catal. B Environ.*, 2012, **125**, 189–196.
70 A. Sellidj and B. E. Koel, *Phys. Rev. B*, 1994, **49**, 8367–8376.
71 W.-Y. Yu, G. M. Mullen and C. B. Mullins, *J. Phys. Chem. C*, 2014, **118**, 2129–2137.
72 F. Gao and D. W. Goodman, *Chem. Soc. Rev.*, 2012, **41**, 8009.
73 R. H. Nibbelke, M. A. J. Campman, J. H. B. J. Hoebink and G. B. Marin, *J. Catal.*, 1997, **171**, 358–373.
74 T. Engel and G. Ertl, in *Advances in Catalysis*, eds. D. D. Eley, H. Pines and P. B. B. T.-A. in C. Weez, Academic Press, 1979, vol. 28, pp. 1–78.
75 D. W. Goodman, *Chem. Rev.*, 1995, **95**, 523–536.
76 F. Gao and D. W. Goodman, *Annu. Rev. Phys. Chem.*, 2012, **63**, 265–286.
77 X. Xu, J. Szanyi and D. W. Goodman, *Catal. Today*, 1994, **21**, 57–69.
78 J. M. Gottfried, K. J. Schmidt, S. L. M. Schroeder and K. Christmann, *Surf. Sci.*, 2003, **536**, 206–224.